Submicrometer Characterization of Surfaces of Epoxy-based Organic–Inorganic Nanocomposite Coatings. A Comparison of AFM Study with Currently Used Testing Techniques

Milena Špírková,[1] Miroslav Šlouf,[1] Olga Bláhová,[2] Tereza Farkačová,[2] Jaroslava Benešová[3]

[1]*Institute of Macromolecular Chemistry, Academy of Sciences of the Czech Republic, 162 06 Prague 6, Czech Republic*
[2]*Faculty of Mechanical Engineering, University of West Bohemia, 306 14 Plzeň, Czech Republic*
[3]*SVUOM Ltd., 170 04 Prague 7, Czech Republic*

ABSTRACT: Surface properties (morphology, hardness) of transparent colorless epoxy-based organic–inorganic nanocomposite coatings were investigated by atomic force microscopy, optical and scanning electron microscopy, nanoindentation, and the Persoz pendulum test. Friction and wear coefficients were obtained from tribological experiments. The influence of mechanical properties and the size, shape, and concentration of additives (colloidal silica particles and montmorillonite sheets) on the measured surface characteristics are discussed. It was found that the highest surface hardness (assigned by nanoindentation, pendulum test or expressed as the scratch resistance) exhibited materials with the glass-transition temperature close to 20°C. Microcopy techniques revealed that surface morphology is influenced by both types of admixtures: on the nanometer scale by colloidal silica particles and on micrometer scale by montmorillonite platelets. Already 1 wt % of montmorillonite increased friction coefficients and wear resistance without distinctive changes of tensile properties. However, the addition of $\sim$ 20 wt. % of silica nanoparticles was necessary for the increase of wear and scratch resistances. © 2006 Wiley Periodicals, Inc. J Appl Polym Sci 102: 5763–5774, 2006

Key words: nanocomposite; coating; atomic force microscopy; sol–gel processes; surface properties; nanoindentation; scratch resistance; pendulum test

INTRODUCTION

Surface morphology and surface properties (hardness, elasticity, resistance, etc.) belong to the most important characteristics of materials, especially of films and coatings, because, in most cases, only a thin surface layer exposed to the air determines the durability, performance, and practical utility of films and coatings used for protecting the less-resistant bulk materials. Several methods of surface hardness measurement have been developed and used.[1–7] All of them require a precise and unambiguous definition of the test conditions, because the surface hardness of thin layers depends not only on the total thickness and the thickness being probed, but also on a number of other factors. In this respect, a fully quantitative characterization of the surface hardness belongs to the ill-defined measuring procedures. In different fields, such as material engineering, material science, polymer chemistry, etc., unified test conditions and criteria have been established, recognized, and accepted by broad communities of researchers and engineers. With the advent, development, and optimization of novel nanoscopic physicochemical techniques, such as atomic force microscopy, in last two decades, interesting new possibilities of characterization of surface properties at the nanometer level arise.[8–15] However, it is not always obvious how the nano-characteristics determined by new techniques translate in macroscopic quantities and how they compare with those measured by methods that probe much larger areas and thicker layers.

In this article, we focus on surface properties of hybrid polymer coatings, formed by silicon-containing precursors and Jeffamines. When studying the surface properties of hybrid organic–inorganic polymeric coatings, the following aspects have to be taken into account. Polymer chains close to the surface (i.e., at distances from the air–polymer interface comparable with dimensions of polymer coils) are more mobile than those in the bulk material. This has been confirmed by measurements of the glass-transition temperature of thin films, T_g, which was found to

decrease with decreasing thickness of the film.[16] In the 3D bulk materials, the properties of the subsurface layer change in the direction perpendicular to the surface and reach constant values at distances exceeding substantially the dimensions of polymer coils. Since the surface layer plays a negligible role in macroscopic materials, the current microscopic techniques, which, in contrast to nanoscopic techniques, probe usually fairly thick layers, yield the bulk properties of materials. However, in the 2D materials, e.g., in coatings and free-standing films, the average properties are strongly affected by the large surface-to-volume ratio. In ultrathin free-standing films, the properties inside the film do not have to reach the corresponding bulk values and the overall mobility of polymer chains may be higher than that in the corresponding 3D bulk material. This, in turn, may affect surface properties and the chains at the surface could be more mobile than those at the surface of bulk materials. To the best of our knowledge, the conformational behavior and mobility of individual chains in thin films have not been studied in sufficient detail.

The dynamic behavior of chains in coatings is even more complex. Because an ideal coating sticks firmly to the support, the mobility of chains in a thin layer adhering to the support is reduced. Hence, the adhesion forces and the properties of the support affect the properties of ultrathin coatings, including the surface properties, while the properties of fairly thick coatings are often less affected by the support.[17–21] The relationship between the surface hardness of thin hybrid O–I coatings and films, which reflects the ability to resist the deformation, and the elasticity, which refers to its capability of reversing deformation and regain its original surface profile, is very complex, depends on the overall thickness and, to the best of our knowledge, has not been much studied and never fully understood and described.

Several years ago, we prepared and characterized an extensive series of O–I coatings and films based on two functionalized organosilicon precursors and three oligomeric amines.[22–24] In some cases, the synthesized coatings also contained colloidal silica particles. Our attention was focused mainly on the structure and segmental dynamics of final films and further on the self-organization and micro- and nanoheterogeneity of the products. We studied the formation of nanostructures as a function of the reaction time under different reaction conditions. We also investigated mechanical properties of selected samples and their relationship to the bulk structure and surface morphology. The solid-state NMR, small-angle X-ray scattering, and atomic force microscopy studies on coatings (analyzed on free-standing, 150 ± 10 μm thick nanocomposite films) revealed: (i) preferential accumulation of added silica particles at the surface and (ii) uniform ordering of nanoparticles in the bulk of the organic–inorganic ma-

trix. The performed studies suggested the possibility of tailoring and controlling the bulk properties of O–I coatings on the nanometer scale. Recently we have been using montmorillonites (MMT) as additives because their different shapes and sizes allow for a larger modification of properties of the composite materials as compared with modifications due to the presence of silica particles.

In this article, we present the first data on the MMT-containing samples. We studied the (i) surface morphology, (ii) surface hardness, and (iii) wear properties using different nano-to-microscopic techniques. The main purpose of the study is twofold: First, we characterized the prepared MMT-containing samples in detail to find the relationship between the composition of the reaction mixture and the reaction conditions used and the properties of final products. This first stage of the research allowed us to select the best samples for different types of applications and elaborate a protocol for their reproducible preparation. Second, we compare results of several tests (e.g., scratch, indentation, and pendulum tests) differing in the way how the force is applied and in the size and thickness of the probed area. The second part of the research is aimed at the relation between results of different techniques probing the surface on the nano- and micrometer scale. The results gained from the surface measurements can also be used in prospective practical applications of coatings as scratch- and abrasion-resistant topcoat layers.

EXPERIMENTAL SECTION

Materials and procedures

[3-(Glycidyloxy)propyl]trimethoxysilane (GTMS, Fluka; code mark in Tables and Figures: G(3)), diethoxy[3-(glycidyloxy)propyl]-methylsilane (GMDES, Fluka; code mark G(2)), oligo(oxypropylene) diamines and -triamine, Jeffamine D-230, D-400, and T-403 (D230, D400, and T403; code marks: D(S), D(L) and T, Huntsman Corp., USA), colloidal silica (SiO$_2$ 40% solution in water; d = 29 nm; Ludox AS-40, Aldrich; code mark Si), montmorillonite Cloisite® Na (particle size: <2 μm (10%); <6 μm (50%); <13 μm (90%), density: 2.86 g/cm^3, MMT, Southern Clay Products, TX; code mark M), propan-2-ol (IP, Lachema, Czech Republic), and hydrochloric acid, 38% (Lachema, Czech Republic) were used as-received.

Functionalized organosilicon precursors (GTMS, GMDES, or GTMS + GMDES) were mixed with water, propan-2-ol, and possibly with colloidal silica particles and stirred for 24 h at ambient temperature. pH of the mixture was adjusted to 4 with dilute HCl. Then a solution of the oligomeric amine in aqueous alcohol was added. The reaction mixture was stirred at ambient temperature for 1 h (samples 3, 5, and 6)

or 2.5 h (1, 2, and 4). Due to the alkaline character of Jeffamine, pH of the resulting reaction mixture increased to 8–9 (in the case of MMT-containing sample, MMT dispersion in water was added and stirred for additional 15 min). Then the reaction mixture was spread on glass or modified polypropylene sheets with constant thickness using a bar coater with a 300-μm gap. The sheets were immediately (or after 15 min for MMT-containing coating) placed into an oven and kept at 80°C (2 h) and 105°C (1 h). The thickness of the final coatings was 150 ± 10 μm. The composition of studied samples and their codes are given in Table I.

Techniques

Atomic force microscopy

All measurements were performed under ambient conditions using a commercial atomic force microscope (MultiMode Digital Instruments NanoScope™ Dimension IIIa). Olympus oxide-sharpened silicon nitride probe (OMCL TR-400, spring constant 0.02 N/m; OTR8, spring constant 0.68 N/m) were used for contact mode measurements. Diamond-coated probe (DT-FMR; spring constant 1.9 N/m) was chosen for tapping and contact modes. In the contact mode for surface morphology determination, the normal forces of the tip on the sample were reduced and did not exceed 20 nN. To study the scratch resistance, the normal forces, applied to the 350 nm length at velocity 4 μm s^{-1} for 30 s were increased up to ∼ 300 nN.

Optical microscopy

Samples were cut off from the membranes and observed in an optical microscope Zetopan Pol (Reichert) equipped with a digital camera DXM1200 (Nikon). The samples examined in reflected light were sputtered with platinum (thickness layer ∼ 4 nm) using a vacuum sputter coater SCD 050 (Balzers) to increase refractive index.

Scanning electron microscopy

Scanning electron microscopy (SEM) microphotographs were obtained with a microscope JSM 6400 (Jeol). All images were obtained in the secondary electron mode at 25 kV. A tilt of 30° was used to enhance surface contrast.

Nanoindentation

Nanoindentation measurements were performed under ambient conditions using an ultra micro hardness tester Shimadzu DUH-202 (Shimadzu Corp., Japan) enabling the load range from 0.1 to 1961 mN with the loading precision ±0.002 mN and indentation from 0 to 10 μm, with a resolution of 0.001 μm. Vicker indenter and maximal load 4.9 mN were used for all experiments.

Pendulum hardness

Pendulum hardness (Persoz type) was measured on the Persoz pendulum Erichsen model 299/300 (SVUOM). The Persoz pendulum rests on two stainless-steel balls of 8 mm diameter (hardness HRC 59) located 50 mm from each other. A counterpoise is not provided. On a reference polished plate–glass panel, the frequency of oscillation was set to 1 s^{-1} and the time for damping the angular displacement from 12° to 4° was 430 s. The total mass of the pendulum is 500 g and its center of gravity at rest is 60 mm below the plane of the fulcrum, the pointer tip is 400 mm below the plane of the fulcrum. The pendulum hardness is defined as the ratio of the number of oscillations of a pendulum on the testing surface versus the reference surface (burnished glass) necessary to achieve tilt damping from 12° to 4°.

Tribology

The friction and wear behavior of selected coatings were tested at ambient temperature on tribometer THT CSEM (CSM Instruments SA, Switzerland) A pin-on-disc principle was used: coating sample deposited on glass is mounted in a holder rotating with a velocity 100 mm s^{-1}. A sphere-shaped pin (steel ball of 6 mm diameter) was loaded with the force of 1 N on the rotating coating sample producing wear track of a given

TABLE I
Composition and Codes of Studied Samples

Sample	SiO$_2$ (wt %)	MMT (wt %)	GTMS (wt %)	GMDES (wt %)	D230 (wt %)	D400 (wt %)	T403 (wt %)	Code
1	21.1	0	47.6	16.0	15.3	0	0	SiG(3)G(2)D(S)
2	19.8	0	58.7	0	21.5	0	0	SiG(3)D(S)
3	20.5	0	0	60.7	0	0	18.8	SiG(2)T
4	0	0	52.2	0	0	47.8	0	G(3)D(L)
5	0	0	0	75.5	0	0	24.5	G(2)T
6	0	1.0	0	75.6	0	0	23.4	MG(2)T

Si, SiO$_2$; M, MMT; G(3), GTMS; G(2), GMDES; D(S), D230; D(L), D400; T, T403.

radius (3.5 mm). The pin ball was mounted on the stiff lever. Friction coefficients between the steel ball and the coating sample (tangential/normal force ratio) were determined from deflections of this lever.

Track formation by a steel ball on the coating surface was measured with a profilometer Hommel Tester T 1000 (Hommelwerke GmbH, Germany) in combination with light microscope Nikon Optiphot 100 S (Nikon Corp., Japan). Wear properties were determined as the volume of coating loss from surface after a friction run (i.e., after 10,000 cycles) due to ball rotation.

RESULTS AND DISCUSSION

Surface morphology and long-time stability

One of the main goals of this article was testing the application of current AFM techniques for studies of the morphology and surface properties of soft hybrid O–I coatings. We wanted to find and optimize conditions for their reproducible use and to test the advantages and limitations of individual measuring modes. First, we employed different AFM techniques for the morphological characterization of soft surfaces differing substantially in the roughness and compared the obtained results. The two main AFM modes, i.e., the contact and soft tapping (dynamic) modes differ substantially in the tip-sample interaction. Further they differ in the resolution and speed and each of them has some advantages and disadvantages. The advantages of the contact mode are: (i) higher scanning velocity and resolution and (ii) the possibility of studying surfaces with sudden and substantial changes in the vertical profile.[25] However, the most important limitation for studying soft surfaces by the contact mode is the fact that the applied force is fairly high and the sharp tip may cause a permanent damage or modification of the surface under investigation. This can distort and obscure the characteristic features of the studied surface. The tapping mode allows for studying very soft surfaces, but its main disadvantage is a very low scanning velocity. For the future application of AFM for the characterization and study of hybrid O–I coatings based on viscoelastic crosslinked matrices, it is important to compare results of both modes for a series of selected samples differing significantly in mechanical properties and to set the limits for the contact mode employment.

Figure 1 shows two 3D scans of the same sample area measured by the DT-FMR probe, which was designed for a multiple scanning of identical spots by both contact and tapping modes. The comparison (for one of fairly soft surfaces) shows that it is possible to use both modes for studying all prepared O–I coatings, because both variants give identical information on the surface morphology. It means that the scratch
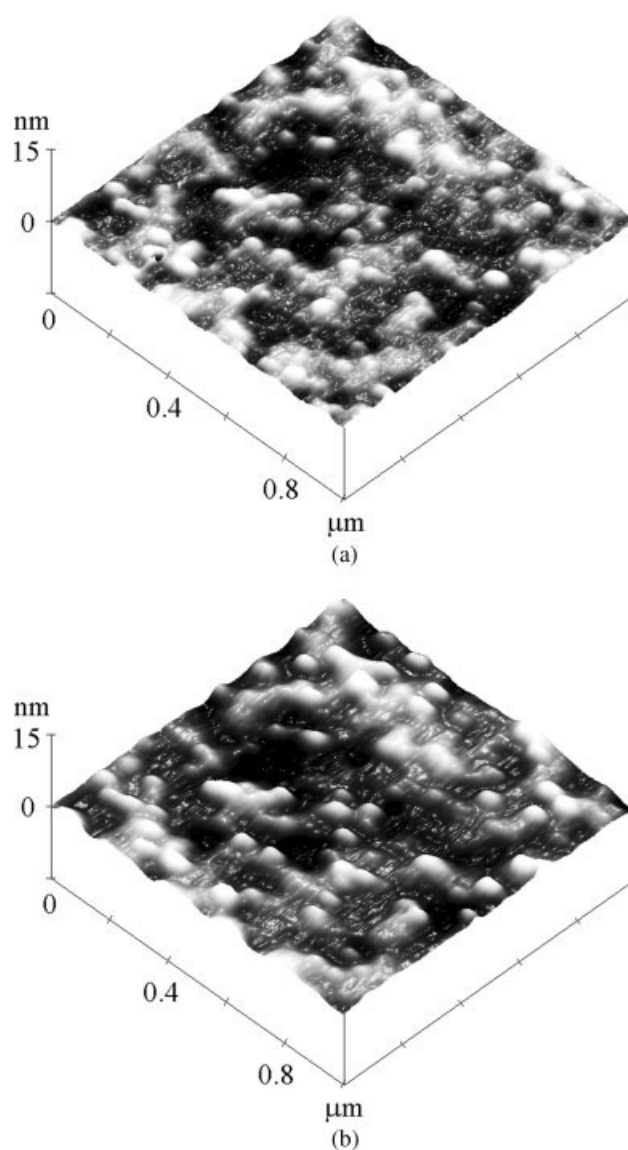

Figure 1 A comparison of results of surface morphology of the identical area of sample 3; code SiG(2)T measured by the DT-FMR probe in the tapping (a) and contact (b) modes.

resistance of all tested coatings is sufficient to resist the forces applied by the AFM tip in the contact mode, i.e., the forces up to 50 nN for individual image measurement. However, to satisfy the condition that the sample surface will not be destroyed by the tip, forces exceeding 20 nN were not used for topography measurements. The study shows that the samples prepared without additives have very smooth and uniform surface (Table II). If the colloidal silica particles are present in the reaction mixture, they are clearly detectable at the surface. They are well-spread and incorporated in the organic–inorganic surface layer without any visible agglomeration. The surface roughness is enhanced as compared with corresponding additive-free coatings (Table II). The study shows that

TABLE II
Roughness Values Determined from AFM Measurements

	Figure no.					
	1a	1b	2a	2b	3d	3e
Sample code	SiG(2)T	SiG(2)T	SiG(2)T	SiG(2)T	MG(3)D(L)	G(3)D(L)
RMS (nm)	0.58	0.66	0.78	0.79	0.28	0.31
R_{max} (nm)	6.01	5.78	8.41	11.6	2.36	2.29

Si, SiO_2; M, MMT; G(3), GTMS; G(2), GMDES; D(S), D230; D(L), D400; T, T403; RMS, root mean square (standard deviation of the z values within a given area); R_{max}, the difference in height between the highest and the lowest points on the surface relative to the mean plane.

the immobilization of silica particles in the organic matrix is fairly strong. A partial covalent bonding of silica particles to the polymeric network has been already proven in our earlier studies by the solid state NMR.[23]

Since the contact AFM mode was found to be a reliable research tool for studying the morphology of coatings, it was used for the examination of surface stability when subjected to climatic conditions. The climatic test consists in a strictly controlled long-term exposure of coatings to humidity at ambient or elevated temperatures. The testing of coatings deposited on Cu, steel, and glass substrates was performed in a climatic chamber (ZKO, SVUOM) under the following conditions: (a) 100% relative humidity, temperature $(38 \pm 2)°C$, exposure up to 300 h; and (b) 80% relative humidity, temperature $(23 \pm 2)°C$, up to 600 h. As it is evident from Figure 2, some changes in surface morphology occurred, but all coatings remained compact and fairly smooth (Table II) and did not show major damages. In the case that they are deposited on glass, they stick fairly well to the supporting substrate after long-term exposures. Even though it is impossible to scan the same surface area before and after the exposure, it is obvious that the roughness remains almost the same after exposure to the test conditions described above. This finding is encouraging for potential practical use of tested coatings as topcoats.

As both the filler-free and colloidal silica particles containing coatings showed very good material properties, including targeted surface properties (e.g., scratch resistance), we recently studied also O–I nanocomposites filled with different types of additives, namely coating with dispersed montmorillonites. Montmorillonites are natural clays from the group of dioctahedral smectites consisting of individual, ~ 1 nm thick aluminosilicate platelets arranged in a regular structure of agglomerated stacks due to electrostatic and van der Waals forces. These stacks can be destroyed, e.g., in water, yielding individual (exfoliated) sheets of high energetic hydrophilic surface and high aspect ratio. Cloisite is the trademark of both unmodified and modified (hydrophobised) montmorillonites. For our purpose, an unmodified natural montmorillonite, Cloisite Na^+ was used because of its hydrophilic nature, similar to that of the reaction system.

Because the MMT and SiO_2 nanoparticles differ significantly both in size and shape (see Experimental), their effects on the coating properties differ. The fairly
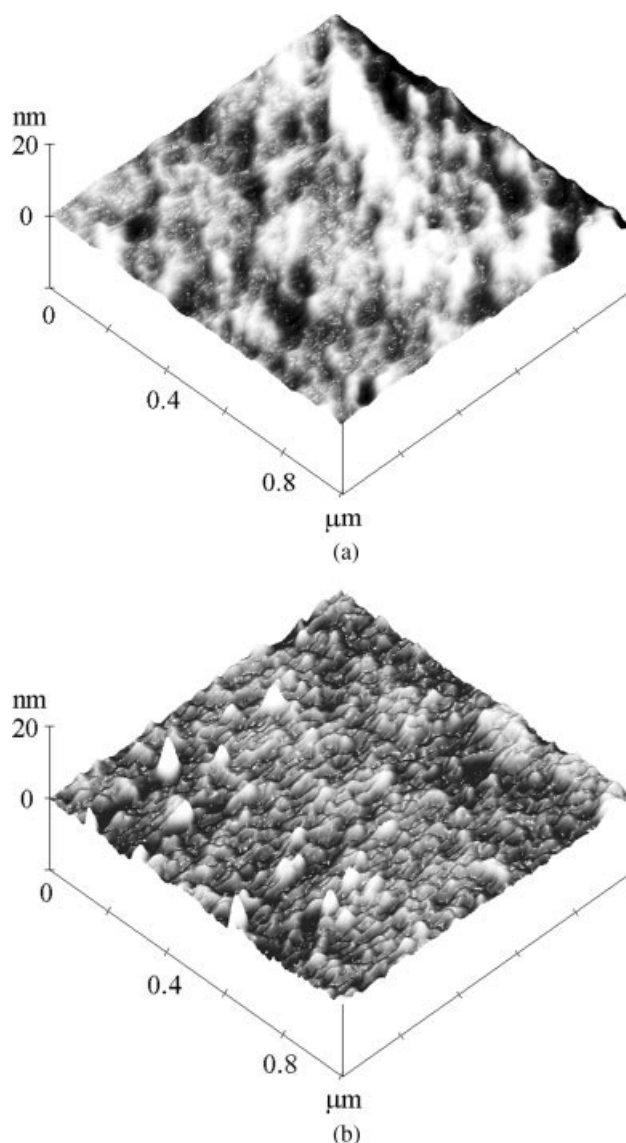

Figure 2 Surface morphology of sample 3; code SiG(2)T deposited on Cu substrate after climatic tests using the contact mode with OMCL TR-400 probe, normal forces < 20 nN. Conditions: (a) 40°C, 100% relative humidity, 167 h; (b) 24°C, 80% relative humidity, 600 h.

large MMT particles start to influence thermomechanical properties of O–I matrices at much lower concentrations than much smaller silica particles. Hence 20 wt % of silica and only 1 wt % of MMT was used to modify the studied coatings. Unlike silica-containing coatings or admixture-free products, the surface morphology of MMT-containing samples is very sensitive to the preparation protocol. MMT particles form clusters of various shape (corrugated, wormlike structures) and size (100–600 μm).[26] An example of MMT-containing coating surface (made from GTMS, D400, and MMT) is shown in Figure 3. Figures 3(a) (SEM)

and 3(c) (optical microscopy, reflected light) show the same sample (the same size). From both figures it is evident [more pronounced in Fig. 3(c)] that the MMT particles form worm-like clusters of the size 10^2–10^3 μm. The detail of SEM picture [Fig. 3(b), 5× zoomed detail as compared with 3(a)] reveals the presence of smaller clusters of size 20–40 μm. When the surface morphology of this sample is measured by AFM on the nanometer scale, i.e., with 3000 times higher resolution as compared with SEM and optical microscopy, the AFM image [Fig. 3(d)] is practically the same as in the case of the admixture-free coating surface
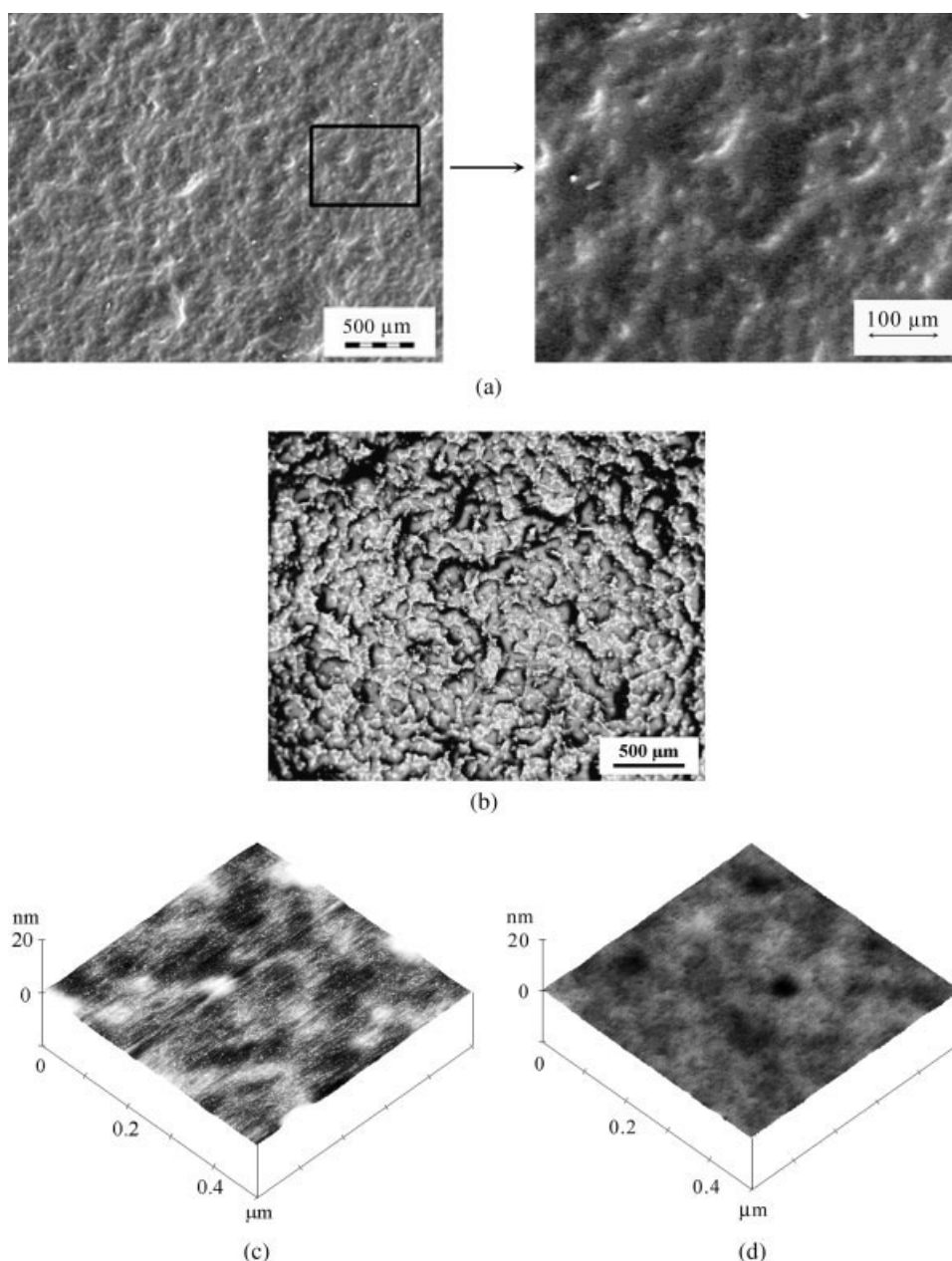

Figure 3 A typical example of surface morphology of MMT-containing coating [made from GTMS, D400, and MMT; code MG(3)D(L)] (a) SEM; (b) detail of Figure 3(a); 5× magnified; (c) optical microscopy in reflected light; (d) AFM in contact mode; (e) AFM image of sample 4; code (G(3)D(L). (OMCL TR-400 probe used for both AFM measurements.)

[Fig. 3(e)]. This proves that the micrometer-size clusters detected by SEM and optical microscopy are due exclusively to the presence MMT sheets in this coating. MMT particles are partially intercalated, and partially exfoliated within the O–I matrix, as detected by WAXS and TEM measurements.[26] It has to be taken into account that while AFM images of coatings without any admixture or with colloidal silica detect morphological motifs of the maximum size of few hundreds of nanometers uniformly distributed on the whole surface, the MMT clusters achieve sizes of tens of micrometers up to units of millimeters which largely exceed the areas of AFM scans. Hence, AFM scan shows only an MMT plate or the MMT-free surface area and can be used only as a supplementary method for studying the surface morphology of MMT-containing samples. The formation of large MMT clusters on the surface of coatings with only 1 wt % of MMT additives suggests that MMT plates concentrate preferentially in the surface region (depending on the conditions used for the coating preparation), although their overall concentration in the reaction mixture is fairly low.

Surface hardness

The surface hardness is usually defined as the resistance to permanent deformation or damage.[1–3] This definition *per se* is not very useful because it requires an additional specification of test conditions. Three basic methods for its evaluation can be used: indentation, scratch, and pendulum test.[17,27–36] They differ in the way how the force is applied and in the size of the tested area. Even though all above techniques became recognized as standard "benchmark" methods of testing materials in industry, they are more or less empirical and it is difficult to compare results obtained for different materials by different methods. During the indentation test, an increasing normal force (i.e., the force perpendicular to the surface) is applied by a sharp tip penetrating in the surface layer and the dependence of the penetration depth versus force per unit surface area is measured. While the evaluation of the indentation test is straightforward, the evaluation of a scratch test is more complex. The scratching is a linear damage caused by a sharp object that irreversibly deforms or perforates the surface. In current practical applications, the damage is performed by a stylus or cutter, and a critical load (fracture threshold) that causes the first observable irreversible damage is measured. When applying and evaluating the scratching, it is necessary to keep in mind that the sharp probe moves parallel with the surface and not only the normal force, but also the tangential force (depending, e.g., on the velocity) play important role. It is not necessary to emphasize that the scratch resistance characteristics cannot be simply compared with those evaluated by methods based on the normal force and that it is difficult to compare results published by different research and industrial groups. A number of theoretical and experimental papers have been published on this subject recently;[27–44] however, the problem of an unambiguous comparison has not been sufficiently resolved yet. The third very common test method used for the characterization of surfaces is the Persoz pendulum analysis.[45] In this case, the damping constant of a pendulum, which "touches" the surface during oscillations, is measured. The method probes a fairly large surface area and a combination of the surface hardness, roughness, and thickness (in the case of a thin coating) affects the results. Despite an enormous difference in the size of tested areas, a common feature of the scratch and pendulum test is the important role of tangential forces. On the other hand, both methods differ in the way how the surface is deformed. The pendulum deformation is usually reversible when applied to viscoelastic materials, while the scratching (similarly to indentation) leads to permanent surface damages.

In this work, we evaluated the surface hardness by all three above techniques and compared the results trying to reveal general features of the surface response to different types of deformation. The tested samples were selected on the basis of results of the mechanical analysis to cover all practically important types of behavior, i.e., the behavior of nanocomposite polymeric materials in the glassy, main transition region and rubbery states at the ambient temperature 23°C. Hence the wide span of thermomechanical characteristics of individual samples, such as the stress at break, strain at break, and toughness, was the main criterion for the selection of tested coatings. Their mechanical properties are given in Table III. Samples 1 and 2 are characterized by a relatively high stress at break, sample 3 is more ductile, but all samples have a relatively high and comparable toughness. It is further evident that samples 1, 2, and 4 exhibit a comparable strain at break, but the toughness of sample 4 is substantially lower than that of samples 1 and 2. For further details concerning the mechanical analysis, see Ref. 24.

Scratch resistance

Atomic force microscopy is a suitable technique for studying the scratch resistance on the nanometer scale. Our study was motivated by the works of Bai et al., Shen et al., and Jones et al.,[46–50] but in contrast to these authors who used the home-made diamond probes with spring constants $\sim$ 300 N/m, we used a commercial contact-mode probe (OTR 8), commonly used only for nondestructive AFM analysis. We have found that the commercial probe (designed for other purposes) is well suited for scratch resistance studies. When an increasing normal force of the tip was

TABLE III
Mechanical Properties of Studied Samples

Sample no.	Code	Stress at break (MPa)	Strain at break (%)	Toughness[a] (MJ/m^3)	T_g[b] (°C)
1	SiG(3)G(2)D(S)	21.6	6.1	0.95	33 (G)
2	SiG(3)D(S)	26.2	9.2	1.5	20 (MT)
3	SiG(2)T	10.7	23.7	1.66	23 (MT)
4	G(3)D(L)	1.8	7.8	0.07	−16 (R)
5	G(2)T	7.3	31.2	1.22	17 (MT)
6	MG(2)T	7.1	26.6	1.01	20 (MT)

Si, SiO$_2$; M, MMT; G(3), GTMS; G(2), GMDES; D(S), D230; D(L), D400; T, T403; G, glassy state; MT, main transition region; R, rubbery state at 23°C.

[a] The energy per volume unit necessary to break the sample.

[b] Glass-transition temperature determined as the maximum of tan δ (from dynamic mechanical thermal analysis).

repeatedly employed on the surface of the sample, the formation of scrapes of different shape and depth was observed depending on the normal force and the number of runs. Figure 4 shows the transition from a nondestructive scanning to a controlled surface destruction scanning, characterized by the formation of grooves.

For a proper evaluation of the scratch resistance from a destructive AFM scan, one has to consider the following model. The scratch resistance is defined as the normal force F_n per unit of the cross section of the area of the scratch A_s, i.e., $S_r = F_n/A_s$.[50] The normal force F_n acting on the surface comprises two contributions: a minority contribution due to attractive capillary forces (in the nanonewton range) and the majority one, controlled by the voltage applied to the piezo element; the latter value depends further on the spring constant of the probe and its sensitivity. The pertinent values of both contributions to the normal force can be obtained from force calibration plots (i.e., from the deflection versus z position dependences) and have to be evaluated for each measurement. The shape of the scratch trace is considered to be a triangle and the scratch area can be obtained by section analysis. In our measurement, the values of A_s used for evaluating the scratch resistance, S_r, are averages of 10 cross sections performed in various positions of the scratch trace. The values of S_r for a given F_n are summarized in Table IV (columns 2 and 3) together with other surface characteristics, and in Figure 5.

The results of surface hardness measured as the scratch resistance lead to following conclusions:

Scratch resistance S_r is not constant, but depends on the applied normal force and decreases with increasing value of F_n. This can be explained by the fact that the brittle fracture, when appears at a certain critical load, starts to prevail over other kinds of damages because it requires less energy as compared with the elastic and plastic parts of deformation, i.e., the fracture continues, but the measured scratch resistance decreases with increasing load.[37]

The products existing at ambient temperature in the main transition region have the highest scratch resistance. The lowest S_r was found for the glassy sample in spite of its considerably high toughness compared with the rubbery one. This can be rationalized by the fact that the rubbery sample exhibits higher elasticity in comparison with the glassy one. We found a relatively good proportionality between the hardness and deformability of the studied coatings in the main transition region.

Comparing samples in the main transition region, which have close values of toughness and temperature of glass transition but differ in stress and elongation at break, the more ductile the sample is, the higher its scratch resistance, e.g., sample 3 has approximately twice higher S_r than the harder sample 2. These conclusions are in accordance with the general finding that, for a given F_n, the scratch resistance increases with increasing elasticity.[50]
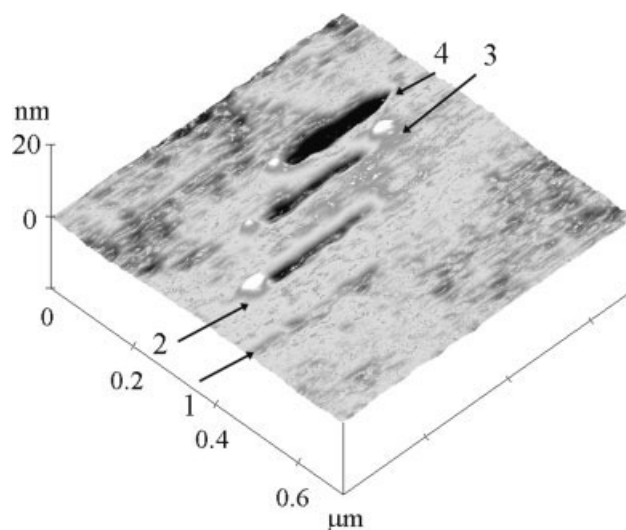

Figure 4 A tilted 3D view of the destructive scan of surface of sample 3; code SiG(2)T. Normal forces 120 nN (1), 177 nN (2), 235 nN (3), and 280 nN (4) applied to the length 350 nm for 30 s at the velocity 4 μm s^{-1}.

<div align="center">

TABLE IV
Surface Properties

</div>

Sample	Code	AFM scratching		Nanoindentation analysis			Pendulum
		F_n (nN)	S_r (GN/m^2)	DHV	h_{max} (μm)	W_p/W_e	Hardness[a] (%)
1	[SiG(3)G(2)S)]G[b]	62	0.072	32 ± 1	0.78	0.66	53.6
2	[SiG(3)D(S)]MT[b]	170	3.5	506 ± 51	0.19	0.46	72.4
		241	2.7				
		367	2.6				
3	[SiG(2)T]MT[b]	120	8.6	288 ± 19	0.26	0.55	70.8
		177	5.9				
		235	5.0				
		280	4.1				
4	[G(3)D(L)]R[b]	104	0.25	2.4 ± 0.2	2.82	0.23	41.3

Si, SiO$_2$; M, MMT; G(3), GTMS; G(2), GMDES; D(S), D230; D(L), D400; T, T403.
[a] Relative to glass.
[b] State at 23°C: G, glassy state; MT, main transition region; R, rubbery state.

Nanoindentation

To compare the surface hardness of coatings, measured by AFM on the submicrometer scale with nanometer penetration depths into the surface with current methods testing surface hardness on larger scales and penetration depths on the micrometer scale, the nanoindentation measurements were also performed. In the benchmark indentation test, the penetration depth, h, is measured as a function of the applied load, P. Indentation curves, for loading (from $P = 0$ to $P = P_{max}$) and unloading (from $P = P_{max}$ to $P = 0$) are shown in Figure 6 for three samples in the glassy, main transition region and rubbery states.

The indentation method yields the Vicker dynamic hardness (DHV) which is calculated from the maximum applied load, P_{max}, and h_{max} (indenter penetration depth at P_{max}), according to the formula DHV $= 37.838 \ P_{max}/h_{max}^2$. Indentation curve gives also information on surface mechanical properties: The total indentation work, W_t, is the area below the loading
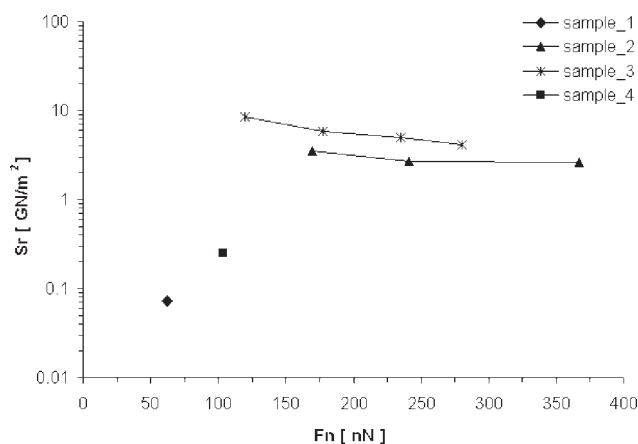
curve. It consists of an elastic component W_e (work under the reverse unloading curve), and plastic part, $W_p = W_t - W_e$. The W_p/W_e ratio is called the plastic-to-elastic index. The values of DHV, h_{max}, and W_p/W_e (averages of 10 measurements) for samples 1–4 are summarized in Table IV (columns 4–6). It is evident, that DHV decreases in the order: main-transition region > glassy > rubbery sample. When comparing DHV of coatings in the main transition region, harder sample 2 has almost twice higher DHV than the more ductile sample 3. As expected, the plastic-to-elastic index decreases in the order glassy > main-transition region > rubbery coating. A rather surprising result is that the more ductile sample 3 has a slightly higher W_p/W_e ratio compared with the harder sample 2, i.e., the sequence is opposite to that for the scratch resistance. This fact could be explained by the presence of different inorganic nanostructures and their different incorporation into the organic matrix. Sample 2 con-
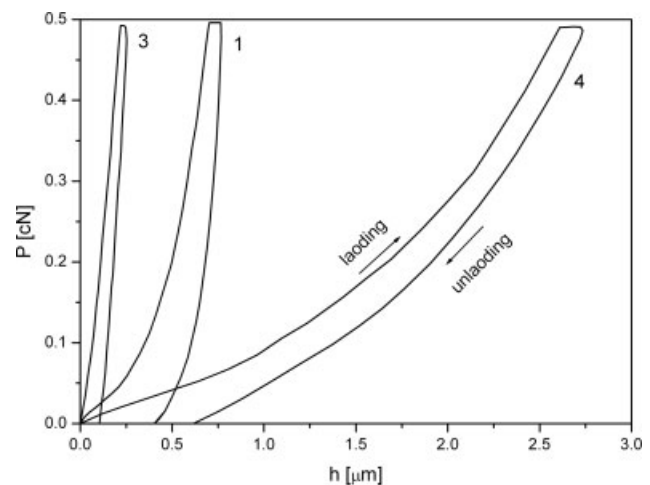

Figure 5 Scratch resistance versus normal force values for samples 1 to 4; codes SiG(3)G(2)D(S), SiG(3)D(S), SiG(2)T, and G(3)D(L).

Figure 6 Indentation curves of samples 1, 3, and 4, codes SiG(3)G(2)D(S), SiG(2)T, and G(3)D(L). All unloading curves are right-shifted to obtain clear plots; $\Delta h = 0.1 \ h_{max}$ for samples 1 and 3 and $\Delta h = 0.05 \ h_{max}$ for sample 4.

TABLE V
Friction and Wear Coefficients

Sample no.	Code	Initial friction coefficient	Stable friction coefficient	Wear coefficient (mm³/Nm)
3	SiG(2)T	0.585	0.925	0.043
5	G(2)T	0.576	0.740	2.015
6	MG(2)T	1.934	2.070	0.577

Si, SiO$_2$; M, MMT; G(3), GTMS; G(2), GMDES; D(S), D230; D(L), D400; T, T403.

tains rigid inorganic clusters formed by the sol–gel process (from GTMS precursor) and organic matrix made by the reaction of glycidyl groups with diamines, while sample 3 contains more elastic inorganic nanostructures (from GMDES precursor) and the epoxy matrix containing three-functional triamine junction points. For further details, see Refs. 22–24.

Pendulum hardness

It is interesting to compare the results of AFM tests performed on nanometer scale with current empirical macroscopic tests used in applied materials science. Such comparison should reveal not only the relation between the nano- (or submicron) and macroscopic properties and tests performed at corresponding scales, but also the advantages and disadvantages of AFM for practical applications. The pendulum hardness test ranks among the most commonly used techniques in material research. The values of Persoz pendulum hardness of tested O–I coatings (the average of three measurements) are summarized in Table IV (column 7). It is evident that pendulum hardness decreases in the order: main transition region > glassy and > rubbery coating. When comparing samples 2 and 3, the order of pendulum hardness is the same as in nanoindentation measurements.

As expected, different techniques of surface hardness determination lead to different results, not only in absolute values but also in the order of samples in individual states (glassy, main transition region, rubber) depending on the kind and mechanism of external forces causing the surface deformation or damage. All tests (scratch, indentation, and pendulum) show that the coatings in the main transition region have the highest surface hardness. The results of individual tests, i.e., the scratch test on one side the two remaining (indentation and pendulum) on the other side, do not compare well for the glassy and rubbery samples: while the rubbery sample 4 has higher scratch resistance than glassy sample 1, the other two techniques indicate the opposite trends as concerns the surface hardness characteristics. The scratch resistance and surface hardness exhibit opposite trends also for samples which differ in tensile strength and elasticity. The more elastic sample 2 shows higher scratch resistance than sample 3, while the sample with a higher strength and a lower elasticity shows higher surface hardness when tested by indentation and pendulum tests. The results suggest that the high surface hardness (expressed as the scratch resistance, nanoindentation or as pendulum hardness) of studied O–I nanocomposite coatings require a compromise between elasticity (deformability) and strength (stiffness). This can be, in our opinion, achieved in a relatively narrow region close to T_g, i.e., for samples with T_g values close to 20°C, it means for coatings in the main transition region. As the final elastic/stiffness properties of studied samples are determined predominantly by the specific character of the O–I matrix and are influenced by a number of factors (length of oligo(oxypropylene) chain, kind, functionality, and ratio of starting compounds, technique of preparation, character of arising inorganic structures, etc.),[22–24] the specific conclusions are valid only for the studied samples. However, the performed study revealed general complexity and partial incompatibility of different approaches used for testing very thin polymer layers and showed that a careful detailed comparative research on a fairly high number of polymeric coatings of different chemical nature will be necessary to solve this interesting and practically important problem without ambiguities.
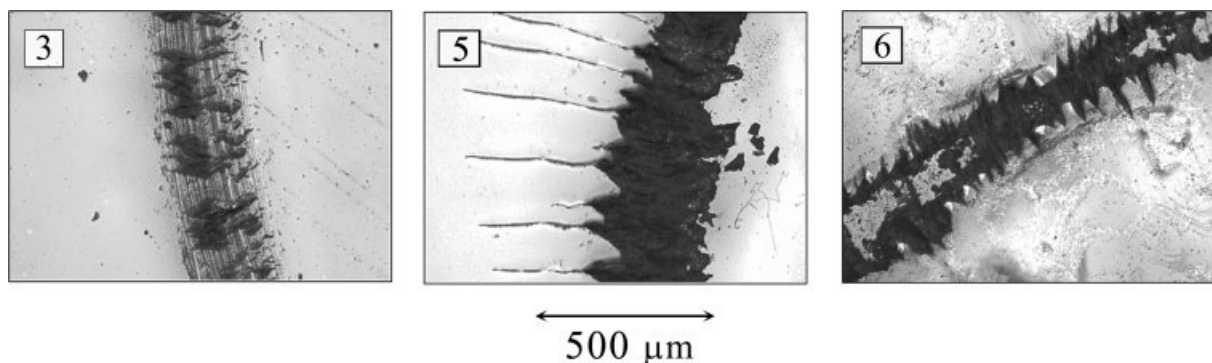

Figure 7 Ball tracks of samples 3, 5, and 6, codes SiG (2)T, G(2)T, and MG(2)T after tribological tests.

Wear properties

To complete the critical evaluation of properties of synthesized coatings and to analyze the influence of the kind, shape and concentration of additives, the common wear properties (i.e., friction and wear coefficients) were tested on three samples: GMDES-T403-SiO$_2$, GMDES-T403, and GMDES-T403-MMT (samples 3, 5 and 6 in Table I). Each sample was measured in five different positions for the determination of friction coefficients and three times for wear coefficient determination. The values given in Table V are average values from these measurements. Wear coefficients were calculated from the volume of the material lost during a specific friction run, $K = V/(L\,s)$, where K is wear coefficient, V is volume of the worn-out material, L is normal load (1 N), and s is ball track.

From Table V it is evident that the coating without any additive shows the lowest friction coefficient. Colloidal silica particles (20 wt %) only slightly increased the friction coefficient; the highest one was found for the sample with MMT. 1 wt % of MMT already considerably influences surface properties of the coating due to considerably higher surface roughness and more complicated surface relief [Fig. 3(a–c)].

The addition of both admixtures improved wear properties (decrease in K values). 1 wt % of MMT has slightly smaller modifying effect just like 20 wt % of SiO$_2$. This can be due either to the low MMT concentration, but more probably due to the fact that if MMT particles are wrenched from the surface, their volume is much higher than that individual SiO$_2$ nanoparticles or O–I matrix abraded from the surface. Figure 7 shows ball tracks of samples 3, 5, and 6 after tribological tests.

CONCLUSIONS

Surface properties (morphology, hardness, wear) of organic–inorganic nanocomposite coatings prepared from silicon-containing precursors and Jeffamines were evaluated by several techniques. It was found that the current atomic force microscopy methods can be used not only for the determination of surface topography but also for the scratch resistance determination. Irrespective of the method used (scratch resistance, nanoindentation or pendulum), it was found that coatings in the main transition region at ambient temperature show the best surface hardness. When comparing coatings in the glassy and rubbery states, the rubbery coatings exhibit better scratch resistances, while glassy samples show higher resistance to nanoindentation and better pendulum test results. The addition of admixtures (20 wt % of colloidal silica or 1 wt % of montmorillonite) improves the wear properties of coatings, namely their abrasion resistance.

The study shows important advantages of AFM for testing thin hybrid nanocomposite films and coatings. The application of different AFM modes enables not only the detailed surface morphology analysis, but also various tests of surface properties on the nanometer scale. A comparison of AFM results with classical tests used in industry revealed that the relationship between nanoscopic and macroscopic test procedures and their results is not always straightforward. It showed that the results obtained by different techniques depend on the thermomechanical state and properties of tested materials (results of all techniques compare well for samples in the main transition region, i.e., close to T_g, but differ for the glassy or rubbery samples). We were able to identify several sources of complications that may occur and should to be avoided. The study on synthesized coatings with inorganic additives showed that added particles may concentrate in the surface layer and particles differing substantially in shape can influence differently the surface and bulk properties and that the onset of the observable influence may occur at very different concentrations.

References

1. Brock, T.; Groteklaes, M.; Mischke, P. European Coatings Handbook; Vincentz Verlag: Hannover, Germany, 2000; p 376.
2. Fink-Jensen, P. Pure Appl Chem 1965, 10, 241.
3. Guevin, P. R. J Coat Technol 1995, 67, 61.
4. Iost, A.; Najjar, D.; Hellouin, R. Surf Coat Technol 2003, 165, 126.
5. Eaton, P.; Estarlich, F. F.; Ewen, R. J.; Nevell, T. G.; Smith, J. R.; Tsibouklis, J. Langmuir 2002, 18, 10011.
6. Fernandes, J. V.; Trindade, A. C.; Menezes, L. F.; Cavaleiro, A. Surf Coat Technol 2000, 131, 457.
7. Ryntz, R. A.; Abell, B. D.; Pollano, G. M.; Nguyen, L. H.; Shen, W. C. J Coat Technol 2000, 72, 47.
8. Zielecka, M.; Bujnowska, E. Prog Org Coat 2006, 55, 160.
9. Wei, Q. F.; Ye, H.; Hou, D. Y.; Wang, H. B.; Gao, W. D. J Appl Polym Sci 2006, 99, 2384.
10. Li, Y. X.; Yang, Y. M.; Yu, F. S.; Dong, L. S. J Polym Sci Part A: Polym Phys 2006, 44, 9.
11. Wang, B. L.; Hu, L. L. Ceram Int 2006, 32, 7.
12. Roche, V.; Vacandio, F.; Bertin, D.; Massiani, Y. J Electroceram 2006, 16, 41.
13. Zheludkevich, M. L.; Serra, R.; Grundmeier, G.; Yang, L. H.; Ferreira, M. G. S. Surf Coat Technol 2006, 200, 4040.
14. He, J. M.; Huang, Y. D. Polym Compos 2006, 14, 123.
15. Alamri, S. N.; Joraid, A. A.; Al-Raqa, S. Y. Thin Solid Films 2006, 510, 265.
16. Blyzniuk, V. N.; Assender, H. E.; Briggs, G. A. D. Macromolecules 2002, 35, 6613.
17. Podgornik, B.; Wanstrand, O. Mater Charact 2005, 55, 173.
18. Kamminga, J. D.; Essen, P.; Hoy, R.; Janssen, G. C. A. M. Tribol Lett 2005, 19, 65.
19. Suyama, S.; Kameda, T.; Itoh, Y. J Mater Sci 2002, 37, 1101.
20. Ceccorulli, G.; Zini, E.; Scandola, M. Macromol Chem Phys 2006, 207, 864.
21. Salvadori, M. C.; Martins, D. R.; Cattani, M. Surf Coat Technol 2006, 200, 5119.

22. Špírková, M.; Brus, J.; Hlavatá, D.; Kamišová, H.; Matějka, L.; Strachota, A. Surf Coat Int B Coat Trans 2003, 86, 187.
23. Brus, J.; Špírková, M.; Hlavatá, D.; Strachota, A. Macromolecules 2004, 37, 1346.
24. Špírková, M.; Brus, J.; Hlavatá, D.; Kamišová, H.; Matějka, L.; Strachota, A. J Appl Polym Sci 2004, 92, 937.
25. Digital Instruments. Scanning Probe Microscopy Training Notebook; Digital Instruments: Santa Barbara, CA, 1998; p 10.
26. Špírková, M.; Brus, J.; Baldrian, J.; Šlouf, M.; Kotek, J. Surf Coat Int B Coat Trans 2005, 88, 237.
27. Heck, G.; Riche, A.; Bardon, J.; Pelletier, H. Z. Metallkd 2005, 96, 1278.
28. Shen, W. D.; Sun, J.; Liu, Z. Q.; Mao, W. J.; Nordstrom, J. D.; Ziemer, P. D.; Jones, F. N.; JCT Res 2004, 1, 117.
29. Bucaille, J. L.; Felder, E.; Hochstetter, G. J. Tribol-T ASME 2004, 126, 372.
30. Mateo, J. L.; Calvo, M.; Bosch, P. J Appl Polym Sci 2005, 98, 163.
31. Tayebi, N.; Conry, T. F.; Polycarpou, A. A. J Mater Res 2003, 18, 2150.
32. Krupicka, A.; Johansson, M.; Hult, A.; Favaro, G. J Coat Technol 2003, 75, 939.
33. Chen, X.; Yan, J.; Karlsson, A. M. Mater Sci Eng A 2006, 416, 139.
34. Barbier, C.; Larsson, P. L.; Ostlund, S.; Hallback, N.; Karathanasis, M. JCT Res 2005, 2, 463.
35. Li, W. Z.; Siegmund, T. Acta Mater 2004, 52, 2989.
36. Puchi-Cabrera, E. S. Surf Coat Technol 2002, 160, 177.
37. Briscoe, B. J.; Sinha, S. K. Materialwiss Werkst 2003, 34, 989.
38. Lim, G. T.; Wong, M. H.; Reddy, J. N.; Sue, H. J. JCT Res 2005, 2, 361.
39. Van Landingham, M. R.; Sung, L. P.; Chang, N. K.; Wu, T. Y.; Chang, S. H.; Jardret, V. D. JCT Res 2004, 1, 257.
40. Shen, W.; Jiang, B.; Scholten, A.; Schwenke, R.; Mi, L.; Seal, C.; Wang, P. Tribol Lett 2004, 17, 637.
41. Gu, X. H.; Nguyen, T.; Sung, L.; Van Landingham, M. R.; Fasolka, M. J.; Martin, J. W.; Jean, Y. C.; Nguyen, D.; Chang, N. K.; Wu, T. Y. JCT Res 2004, 1, 191.
42. Jardret, V.; Lucas, B. N.; Oliver, W.; Ramamurthy, A. C. J Coat Technol 2000, 72, 79.
43. Sundararajan, S.; Bhushan, B. J Mater Res 2001, 16, 437.
44. Wong, M.; Lim, G. T.; Moyse, A.; Reddy, J. N.; Sue, H. J. Wear 2004, 256, 1214.
45. ASTM. Standard test methods for hardness of organic coatings by pendulum damping test; 1995. ASTM D 4366.
46. ISO. Paints and varnishes—Pendulum damping test; 1998. ISO 1522.
47. Bai, M. W.; Kato, K.; Umehara, N.; Miyake, Y.; Xu, J. G.; Tokisue, H. Surf Coat Technol 2000, 126, 181.
48. Shen, W. D.; Jiang, B.; Gasworth, S. M.; Mukamal, H. Tribol Int 2001, 4, 142.
49. Jones, F. N.; Shen, W.; Smith, S. M.; Huna, Z.; Ryntz, R. A. Prog Org Coat 1998, 34, 119.
50. Shen, W.; Ji, C.; Jones, F.; Everson, M. P.; Ryntz, A. Surf Coat Int 1996, 79, 253.